Laser and Particle Beams (2009), *27*, 115–122. Printed in the USA.

doi:10.1017/S0263034609000172

Investigations of plasma jet interaction with ambient gases by multi-frame interferometric and X-ray pinhole camera systems

A. KASPERCZUK,[1] T. PISARCZYK,[1] PH. NICOLAI,[2] CH. STENZ,[2] V. TIKHONCHUK,[2] M. KALAL,[3] J. ULLSCHMIED,[4] E. KROUSKY,[5] K. MASEK,[5] M. PFEIFER,[5] K. ROHLENA,[5] J. SKALA,[5] D. KLIR,[6] J. KRAVARIK,[6] P. KUBES,[6] AND P. PISARCZYK[7]

[1]Institute of Plasma Physics and Laser Microfusion, Warsaw, Poland
[2]Centre Lasers Intenses et Applications, Universite Bordeaux, Talence, France
[3]Czech Technical University in Prague, FNSPE, Prague, Czech Republic
[4]Institute of Plasma Physics AS CR, Prague, Czech Republic
[5]Institute of Physics AS CR, Prague, Czech Republic
[6]Czech Technical University in Prague, FEE, Prague, Czech Republic
[7]Warsaw University of Technology, ICS, Warsaw, Poland

(RECEIVED 7 September 2008; ACCEPTED 2 December 2008)

Abstract

Interactions of laser driven plasma jets with He and Ar gas puffs was investigated experimentally by means of three-frame interferometric/shadowgraphic system and three-frame X-ray pinhole camera. A defocused iodine laser beam using the Prague Asterix Laser System (PALS) interacting with massive planar Cu targets generated high-speed well-collimated plasma jets. The PALS third harmonic (0.438 μm), with pulse duration of 250 ps (full width at half maximum), and energy of 100 J was employed in two irradiation geometries: with an incidence *normal* to the target surface and with an *oblique* one (30° with respect to the target normal), in order to minimize the heating of the ambient gas by the laser beam. The results of these interaction experiments, in particular, those obtained in case of the oblique incidence geometry, are presented and discussed. They show the effect of the double shock formation in ambient gases: starting by the ablative plasma action, followed by that of the jet.

Keywords: Ambient gas; Plasma jets; Shock waves; Three-frame interferometry/shadography

INTRODUCTION

Collimated plasma outflows and jets are of great interest when studying astrophysical phenomena (Remington *et al.*, 2006; Lebedev *et al.*, 2002), as well as simulation of plasma jets generated from different materials in a multi-shell target geometry (Kasperczuk *et al.*, 2008; Schaumann *et al.*, 2005; Sizyuk *et al.*, 2007; Goldman *et al.*, 1999; Blue *et al.*, 2005). Possibilities to have such plasma jets readily available under laboratory conditions would allow many original experiments to be performed. The first successful attempts to generate laboratory plasma jets relevant to astrophysical observations were described recently (Farley *et al.*, 1999; Shigemori *et al.*, 2000). Conically shaped targets made of different materials were irradiated by five beams using a Nova laser, with pulse duration of 100 ps, and 225 J of energy in each beam, or by six beams using a GEKKO-XII laser, with the same pulse duration, but with a total energy of 500 J. In the above-mentioned experiments, the jet-like structures were formed by the cumulative effect of the ablated flows at the axis of conical targets.

Recently, a simpler method for plasma jets production was developed at the Prague Asterix Laser System (PALS) (Jungwirth, 2005; Kasperczuk *et al.*, 2008). It was demonstrated that a partially defocused single laser beam (having its focal plane positioned inside the target), with an interaction spot radius ∼300 μm, energy ∼100 J of the third harmonic (0.438 μm), and a pulse duration of ∼250 ps (full width at half maximum), interacting with a massive planar metallic target (with relatively high atomic number) could produce plasma jets with very interesting parameters

Address correspondence and reprint requests to: Milan Kalal, Czech Technical University in Prague, FNSPE, Brehova 7, 115 19 Prague 1, Czech Republic. E-mail: kalal@fjfi.cvut.cz

(Kasperczuk *et al.*, 2006, 2007*a*, 2007*b*). In our previous studies, the plasma jets were always created at the normal incidence of the laser beam on a massive Cu target. These jets featured a maximum length of 4 mm, a diameter of 300–400 μm, an initial velocity of up to 7×10^7 cm/s, and an electron density above 10^{19} cm^{-3}. In Figure 1, the sequence of shadowgrams, interferograms, and electron equidensitograms illustrates the temporal evolution of such typical plasma jets generated from a Cu planar target.

In order to avoid (or at least to minimize) any direct contact of the heating laser beam with the gas cloud, some changes in the experimental geometry were necessary. The heating laser beam incidence of 30° with respect to the target surface normal was found to be an optimum, which could be achieved under given experimental conditions. This geometry proved to be a necessary prerequisite for the realization of subsequent series of experiments devoted to jet interaction with an ambient media. Experiments performed to verify the plasma jet generation in this new geometry clearly demonstrated that also at the *oblique* incidence the well-formed plasma jets of parameters not worse than those achieved at the *normal* incidence. It might be worthwhile noting that this result is an original finding—so far unpublished.

Parameters of the experimentally produced jets in laboratories differ vastly from those observed in the Universe. For comparison, the parameters of astrophysical jets (Remington *et al.*, 2006; Lebedev *et al.*, 2002) are as follows: length 10^{17}–10^{24} cm, radius 3×10^{15} cm, velocity $(1–5) \times 10^7$ cm/s, and density 10–100 cm^{-3}. However, potential applications of the experimentally produced plasma jets for simulation of astrophysical phenomena require consideration of certain dimensionless jet parameters, namely: (1) The internal Mach number (jet velocity/sound speed inside the jet: $M_{\rm int} = v_{\rm jet}/c_{\rm s(jet)}$)—a high Mach number leads to a reduction of the level of tip broadening due to the Kelvin-Helmholtz instabilities of the interacting surface. (2) The cooling parameter (cooling length/jet radius: $\chi = L_{\rm cool}/R_{\rm jet}$)—an increase of the radiative cooling, i.e., χ results in an increase of the jet density and collimation. (3) The jet-to-ambient density ratio: $\eta = \rho_{\rm j}/\rho_{\rm a}$.

The values of the above parameters for the observed astrophysical jets (Remington *et al.*, 2006; Lebedev *et al.*, 2002) and for the laboratory jets produced in our experiments (Nicolai *et al.*, 2006) are collected in Table 1.

Comparison of values of the above dimensionless parameters between plasma jets produced in the laboratory and the astrophysical ones suggests certain possibilities of laser-produced plasma jets application for simulation of astrophysical phenomena.

EXPERIMENTAL SET-UP AND CONDITIONS

The experiment was performed under the same target irradiation conditions as those mentioned above. To ensure

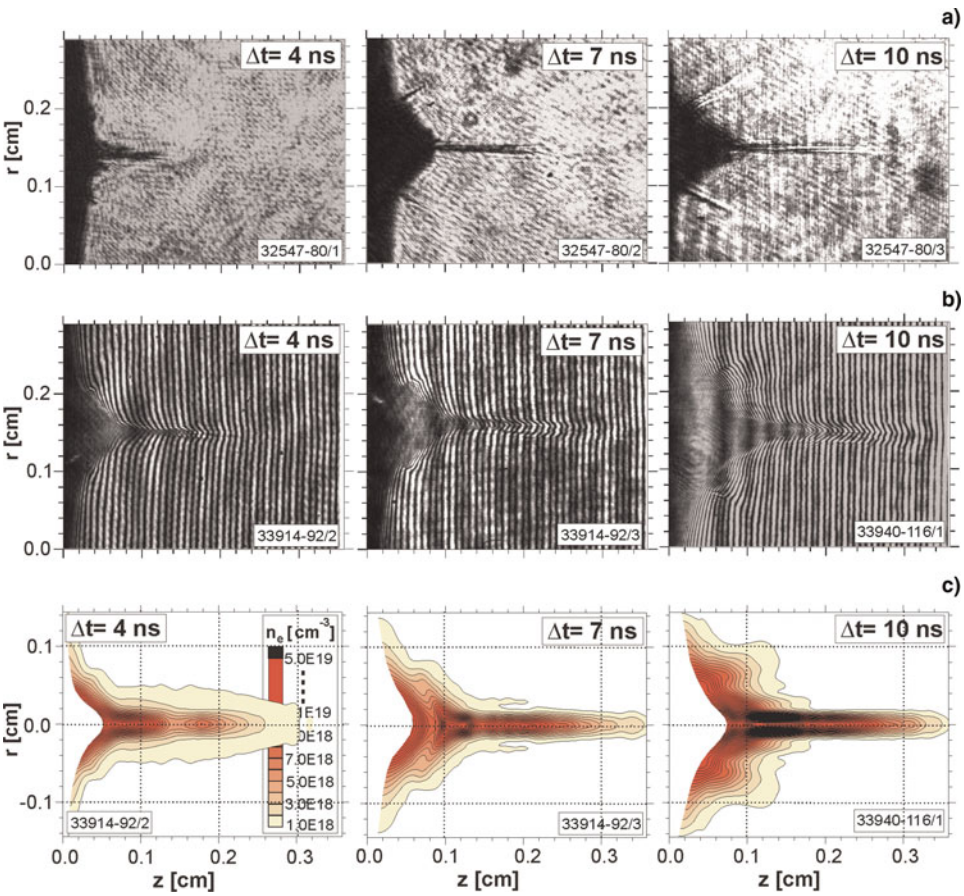

Fig. 1. (Color online) Sequences of shadowgrams, Interferograms, and electron equidensitograms illustrative of the typical plasma jet generated from a Cu planar target.

https://doi.org/10.1017/S0263034609000172 Published online by Cambridge University Press

Table 1. *Comparison of dimensionless parameters for astrophysical and laboratory jets*

	Astrophysical jet	Laboratory jet
Internal Mach number: M_{int}	>10	15
Cooling parameter: χ	≤1	0.1–1
The density ratio: η	≥1	0.1–10

the efficient interaction of these plasma jets with the gas, as an ambient medium, a high-pressure (1–40 bars) supersonic gas nozzle was employed. This device created a cylindrical column of Ar or He neutral gas jets with typical radius of 3 mm. The column axis was parallel to the target surface and separated from the target surface by 3.5 mm. The gas density had a flat-top profile with a plateau of maximum density inside of 1.5 mm radius surrounded by a 1.5 mm smooth gradient. Neutral atom densities varied from 2×10^{17} to 8×10^{18} cm^{-3}. Variations of the gas atomic number and the gas pressure made it possible to control the plasma jet to ambient gas density ratio in the range of 0.1–10. In the first part of the experiment, a normal incidence of the laser beam to the target surface was used. Next, to minimize the interaction of the laser beam with the gas target and its premature ionization, the angle of incidence was changed to an oblique one, 30° with respect to the target surface normal. Positions of the gas puff, together with the heating laser beam (both at the normal as well as the oblique incidence), are schematically outlined in Figure 2. The three-frame interferometric/shadowgraphic system was using the third harmonic (0.438 μm). The three-frame X-ray pinhole-camera with a pinhole diameter of 80 μm registered soft X-ray radiation from plasma in the range of 10–1000 eV. The exposure time of the X-ray camera was set to 4 ns.

COMPARISON OF THE EXPERIMENTAL RESULTS FOR THE NORMAL AND OBLIQUE INCIDENCES OF THE LASER BEAM

Illustrative results of the plasma jet action on a 5 bars Ar gas cloud registered by the X-ray pinhole-camera for both laser beam incidence angles are presented in Figure 3. The action of the plasma jet on the gas results in the creation of a shock wave in the gas column. The created complex plasma structure is characterized by the sharp elongated peak on the axis of symmetry. The images for both incidences geometries are very similar because the X-ray camera registers only radiation from the hot plasma regions.

For comparison, the sequences of shadowgrams (Fig. 4) and electron density distributions (Fig. 5), demonstrating the interaction of the plasma jet with the Ar cloud at the same gas initial pressure as the *normal* and *oblique* laser beam incidence are presented.

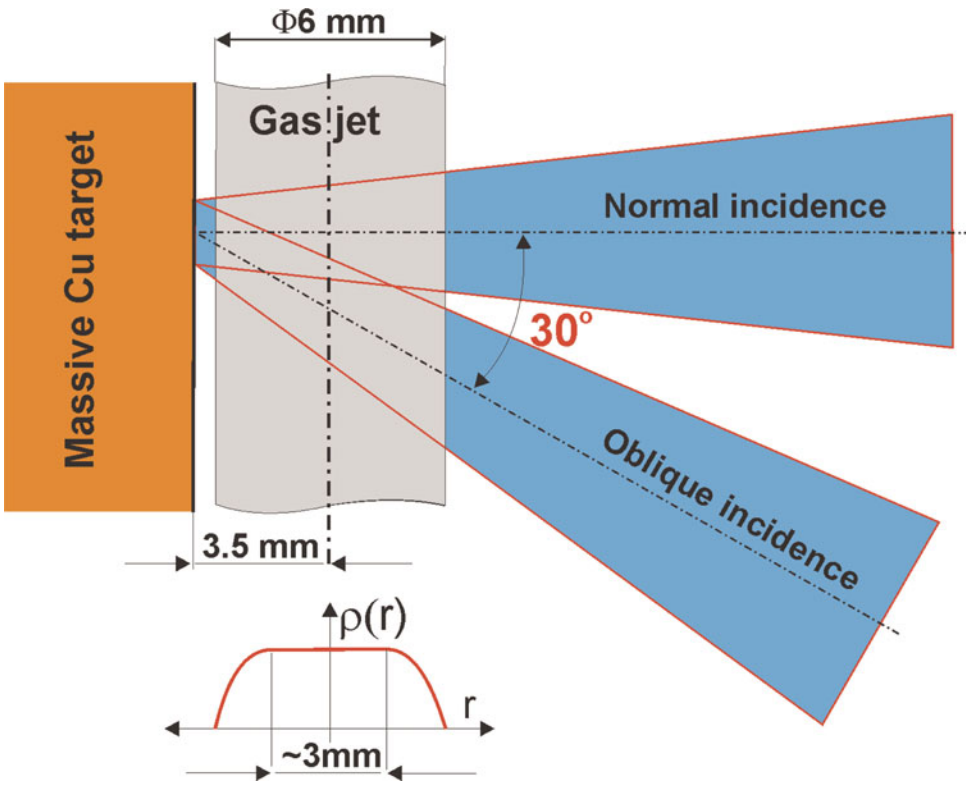

Fig. 2. (Color online) Schematic illustration of the target irradiation for two incidence geometries of the laser beam and positions of the gas puff with respect to the target surface. The corresponding neutral gas density distribution is shown at the bottom.

https://doi.org/10.1017/S0263034609000172 Published online by Cambridge University Press

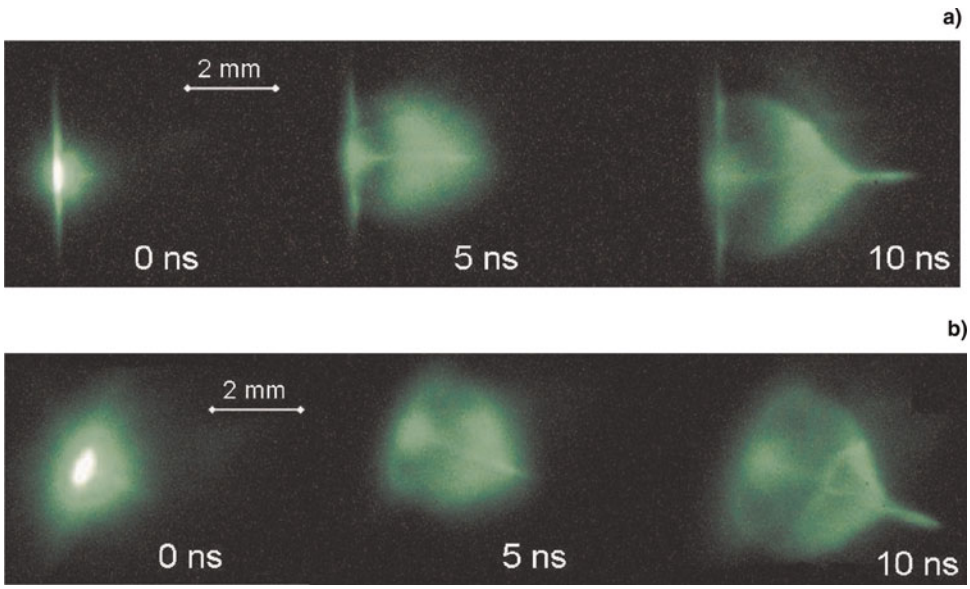

Fig. 3. (Color online) Sequences of X-ray images recorded for the same conditions as described in Figure 1 captions—but at slightly different delays (side views): the *normal* laser beam incidence (**a**) and the *oblique* incidence (**b**).

One can see that shadowgrams (recording only strong gradients of electron density) are also very similar for both incidence geometries. These strong electron density gradients correspond to the plasma jet and the shock wave induced by it.

Information about processes taking place in the gas cloud ahead of the shock wave could be obtained from interferograms. Differences in the electron density distributions, as seen in Figure 5, result from the action of the laser beam on the gas target. In the case of the normal incidence, the heating laser beam is passing directly through the gas column before reaching the target, and strongly disturbs the gas target itself. This is shown in Figure 5a, where the Ar ionization by the heating laser beams preceding the plasma jet formation is clearly visible (emphasized by the blue dashed line in the second picture denoting the laser caustic boundaries).

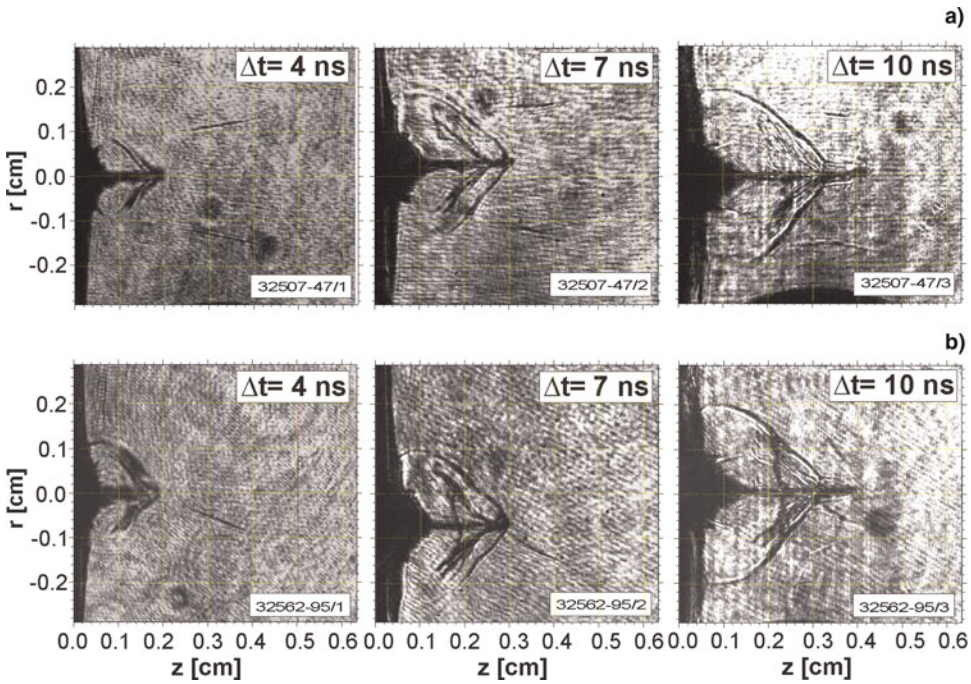

Fig. 4. (Color online) Sequences of shadowgrams illustrative of the interaction of the plasma jet with the Ar cloud at the gas initial pressure of 5 bars for the *normal* (**a**) and the *oblique* (**b**) laser beam incidence geometries.

https://doi.org/10.1017/S0263034609000172 Published online by Cambridge University Press

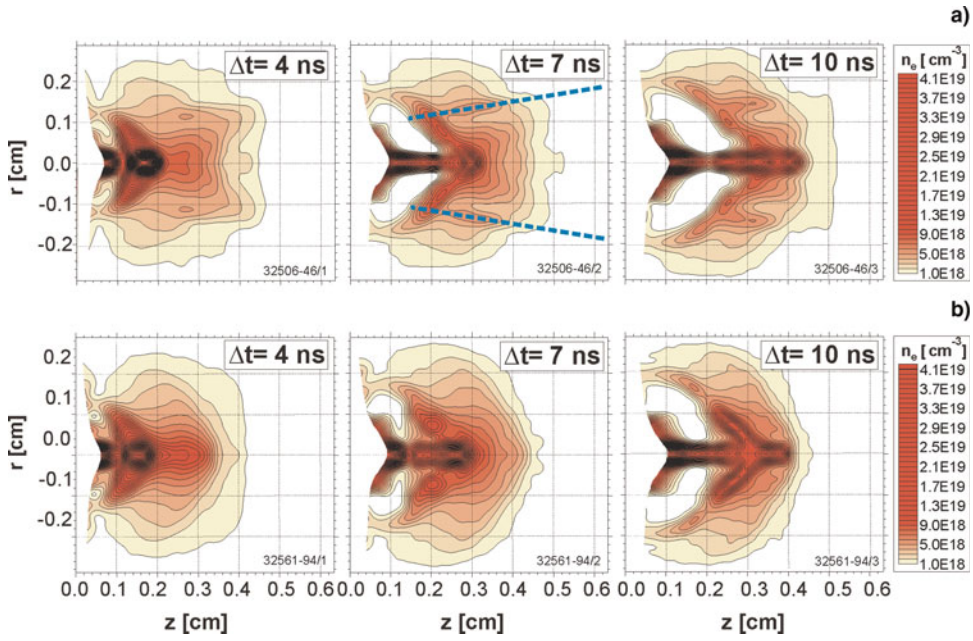

Fig. 5. (Color online) Sequence of electron distributions illustrative of the interaction of the plasma jet with the Ar cloud at the gas initial pressure of 5 bars for the *normal* laser beam incidence (**a**) and the *oblique* incidence (**b**). The dashed line corresponds to the laser beam *caustic*.

DISCUSSION OF PROCESSES ACCOMPANYING THE INTERACTION OF THE PLASMA JET WITH AMBIENT GASES

Processes accompanying the interaction of the laser-produced plasma jet with ambient gas can be observed most distinctly in the case of Ar, at the highest pressure used for this gas (10 bars). They run slower with higher intensity than in Ar at lower pressures or in He. In Figure 6, a corresponding sequence of the plasma configurations is presented in the form of spatial electron densities and electron equidensitograms.

In the plasma jet-ambient gas interaction, the following three stages could be identified: (1) ablative plasma generation and preliminary ionization of the ambient gas (Beilis, 2007), (2) creation of the first shock wave in the ambient gas (Johzaki *et al.*, 2007; Kolacek *et al.*, 2008; Ramis *et al.*, 2008; Yu *et al.*, 2007), and (3) plasma jet forming and the second shock wave generation.

The First Stage

Generation of the ablative plasma on the surface of the Cu target induces thermal X-ray emission, which partially ionizes the ambient gas. The oval-shaped plasma configuration created in front of the target, shown in Figure 4b, with its border represented by the electron density contour $n_e = 10^{18}$ cm^{-3}, corresponds to the plasma created by an action of the thermal X-ray radiation on the gas target. One can see that this plasma covers the whole area taken by the gas-puff and spreads axially up to 5 mm from the target surface. To estimate the degree of ionization caused by the above mechanism, the following line of reasoning could be used: Ar at the pressure of 10 bars corresponds to the neutral atom density at the plateau of the gas jet 2×10^{18} cm^{-3}. From the region in the gas jet adjacent to the area affected later by the incoming plasma jet, the electron density $n_e \approx 8 \times 10^{18}$ cm^{-3} can be determined. Hence, the average charge of the Ar ions in this region should be $Z \approx 4$ and the thermal X-ray emission is, at this stage, the most influential ionizing mechanism. This stage lasts until the first shock wave inside the gas target is generated.

The Second Stage

The first shock propagating into the ionized gas results from the ablative plasma action on the gas target, i.e., it precedes the plasma jet creation. This process corresponds to that described earlier (Arnold *et al.*, 1999; Wen & Mao, 2007), where an analytical model of the hemispherical plasma expansion into an ambient atmosphere is presented. Namely, in the presence of ambient gas, the plasma plume acts as a piston. The ambient gas is compressed and heated by an external shock wave. At the same time the ambient gas acts on the plume and heats it up. The heating starts near the contact surface, where the ions of the plume collide with the ambient gas molecules and are reflected back. The internal shock wave is formed there and propagates inward. At a certain distance from the target, the plasma plume stops, while the external shock wave weakens and degenerates into a sound wave.

https://doi.org/10.1017/S0263034609000172 Published online by Cambridge University Press

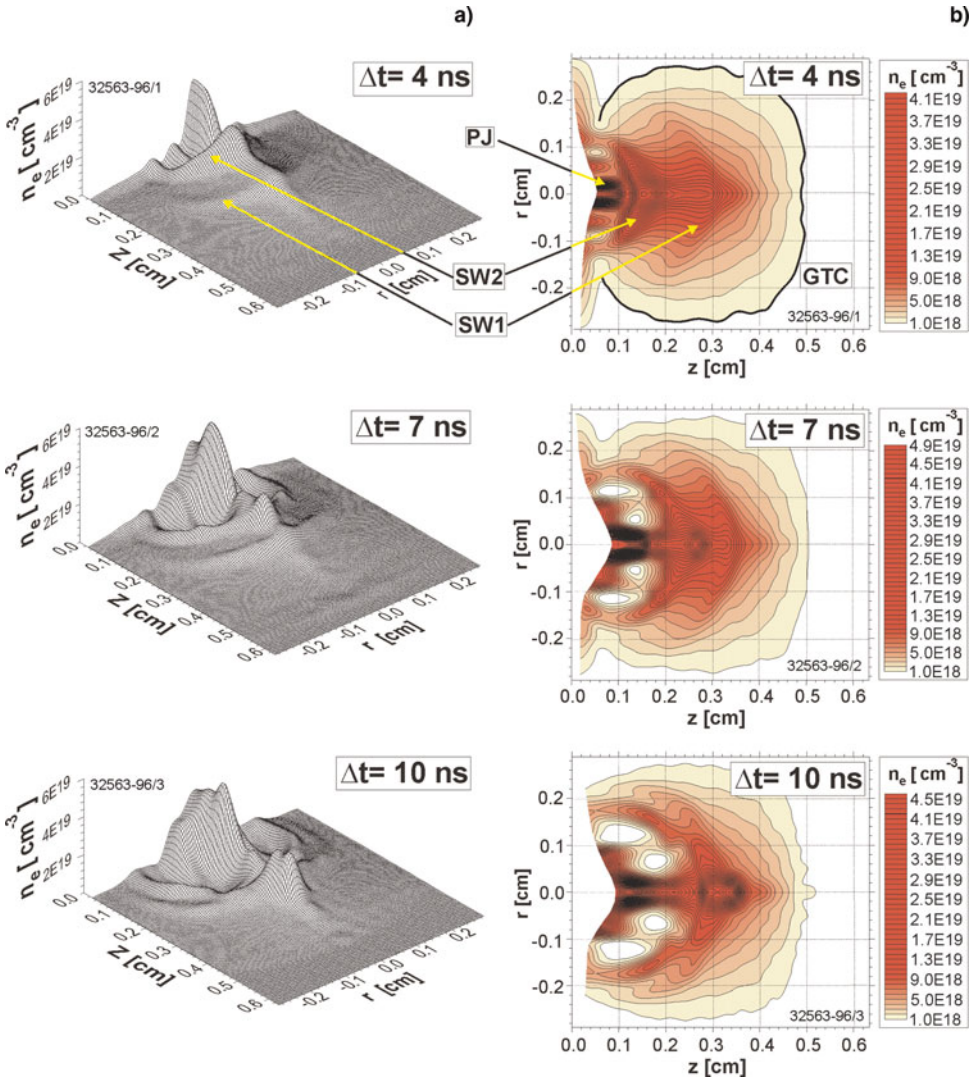

Fig. 6. (Color online) Sequence of electron density distributions for Ar at a pressure of 10 bars in spatial (**a**) and equidensitogram (**b**) form. Denotations: gas target contour (GTC), plasma jet (PJ), the first shock wave (SW1), and the second shock wave (SW2).

The above description concerns the complete process of the plasma plume interaction with an ambient medium. In our case, however, due to a relatively small diameter of the gas-puff, only the initial part of this process could be observed, i.e., until the shock wave reaches the gas-puff more distant outer edge. At the Ar pressure of 10 bars, the velocity of the first shock is rather small ($\sim 0.7 \times 10^7$ cm/s), so its propagation is clearly visible.

The Third Stage

The third stage is connected with the plasma jet creation and its action on the ambient plasma located behind the first shock. The plasma jet creation is delayed by ~ 2 ns after the laser action. In the case of the plasma expansion into vacuum, the plasma jet length increases during the first 5 ns with the velocity of up to 7×10^7 cm/s. Next, the axial motion of the jet is stopped, reaching its maximum length about 6 ns after its evolution started. The presence of the ambient medium hampers the jet motion. The interaction of the plasma jet with the ambient plasma results in the generation of the second shock wave with the velocity of about 2.5×10^7 cm/s. The second shock wave catches up with the first one about 10 ns after the laser action (corresponding to the third frame in Fig. 6).

In the case of Ar at a pressure of 5 bars (see Fig. 5b), the gas target with the border at the level of 10^{18} cm^{-3} covers a much smaller area. Due to the lower gas density (pressure), the first shock wave travels faster (with the velocity of about 1.0×10^7 cm/s), than in the case of higher gas pressures, and after 7 ns it is reaching the gas target more distant outer edge. At the same time, the second shock wave with the velocity of 3.5×10^7 cm/s collides with the first one at the gas target border. One can notice elongated shapes of the tips of both shock waves. Explanation of this bow

https://doi.org/10.1017/S0263034609000172 Published online by Cambridge University Press

shape of the shock waves can be found in Mizuta *et al.* (2002), where the numerical analysis of cumulative plasma jets produced by intense laser beams interacting with cone targets is presented. When the plasma expands into vacuum, at certain distance from the target, the plasma jet starts spreading out in all directions. In the case of the plasma jet propagation into the ambient gas, the shocked ambient gas slows the jet expansion in the direction perpendicular to the axis of symmetry. As a result of this mechanism, the narrow plasma jet structure is preserved also in the region in which it would normally start breaking up (i.e., when expanding into vacuum).

When He is used as the gas target, the gas puff area visualization is considerably different. Even for the maximum pressure employed (20 bars, which corresponds to the neutral atom density at the plateau of the gas jet of 4×10^{18} cm^{-3}), the preliminary ionization of He is not able to create electron densities sufficiently high to produce phase shifts detectable by our interferometric measurements (Fig. 7). It should be noted that with the set of parameters typical for this experiment, the interferometry recording system allows to resolve the electron plasma densities at the level $n_e = 2 \times 10^{17}$ cm^{-3}. This gives some idea about the He ionization degree upper limit.

Due to the low level of ionization, the He gas target is not visible until the shock wave is generated. Only the compressed and heated gas behind the shock reaches electron density levels, which are sufficient for interferometric observation. In Figure 7, one can see that the amount of plasma grows in time simultaneously with the increasing surface of the shock. The initial distance between the first and the second shock is very small, so that the shock waves combine together in a short time. Since the second shock wave is faster, it further compresses the first one. As a result, the thickness of this composed shock wave region decreases whereas its electron density increases.

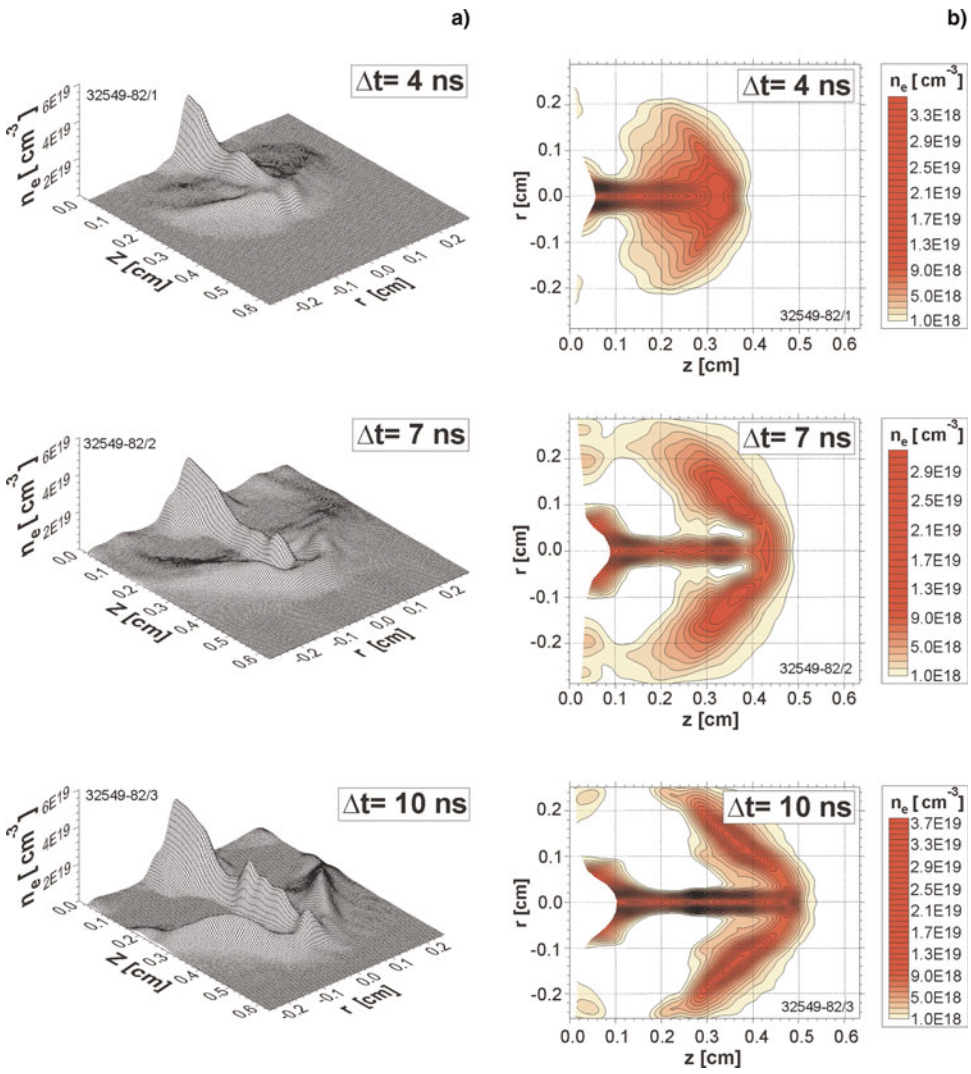

Fig. 7. (Color online) Sequence of electron density distributions for He at a pressure of 20 bars in spatial (**a**) and equidensitogram (**b**) form.

https://doi.org/10.1017/S0263034609000172 Published online by Cambridge University Press

CONCLUSIONS

Our investigations have shown that the very easy method of plasma jet generation, unfolded by us recently at PALS, might open potential possibilities of plasma jet applications in original physical experiments. This work has also proved that plasma jets of interesting parameters can be produced at both normal and oblique incidence of the heating laser beam on the target. The possibility of the creation of plasma jets of high quality also at the oblique incidence allowed us to minimize the unwanted interaction of the heating laser beam with the gas target (impossible to avoid at normal angle of incidence). Thus, a much more reliable observation of processes accompanying the plasma jet-ambient gas interaction became accessible.

ACKNOWLEDGEMENTS

The work was supported in part by the Polish Ministry of Science and Higher Education (project No. N N202 076635), by the Access to Research Infrastructures activity in the 6FP of the EU (contract RII3-CT-2003-506350, Laserlab Europe), as well as the HiPER project (grant agreement No. 211737), and by the IAEA Research Contract No. 13781.

REFERENCES

Arnold, N., Gruber, J. & Heitz, J. (1999). Spherical expansion of the vapor plume into ambient gas: An analytical model. *Appl. Phys. A* **69**, S87–S93.

Beilis, I.I. (2007). Laser plasma generation and plasma interaction with ablative target. *Laser Part. Beams* **25**, 53–63.

Blue, E., Weber, S.V., Glendinning, S.G., Lanier, N.E., Woods, D.T., Bono, M.J., Dixit, S.N., Haynam, C.A., Holder, J.P., Kalantar, D.H., MacGowan, B.J., Nikitin, A.J., Rekow, V.V., Van Wonterghem, B.M., Moses, E.I., Stry, P.E., Wilde, B.H., Hsing, W.W. & Robey, H.F. (2005). Experimental investigation of high-Mach-number 3D hydrodynamic jets at the National Ignition Facility. *Phys. Rev. Lett*. **94**, 095005-1/095005-4.

Farley, D.R., Estabrook, K.G., Glendinning, S.G., Glenzer, S.H., Remington, B.A., Shigemori, K., Stone, J.M., Wallance, R.J., Zimmerman, G.B. & Harte, J.A. (1999). Stable dense plasma jets produced at laser power densities around 10^{14} W/cm^2. *Phys. Rev. Lett*. **83**, 1982–1985.

Goldman, S.R., Caldwell, S.E., Wilke, M.D., Wilson, D.C., Barnes, C.W., Hsing, W.W., Delamater, N.D., Schappert, G.T., Grove, J.W., Lindman, E.L., Wallance, J.M. & Weaver, R.P. (1999). Shock structuring due to fabrication joints in targets. *Phys. Plasmas* **6**, 3327–3336.

Johzaki, T., Sakagami, H., Nagatomo, H. & Mima, K. (2007). Holistic simulation for FIREX project with FI3. *Laser Part. Beams* **25**, 621–629.

Jungwirth, K. (2005). Recent highlights of the PALS research program. *Laser Part. Beams* **23**, 177–182.

Kasperczuk, A., Pisarczyk, T., Kalal, M., Martinkova, M., Ullschmied, J., Krousky, E., Masek, K., Pfeifer, M., Rohlena, K., Skala, J. & Pisarczyk, P. (2008). PALS laser energy transfer into solid targets and its dependence on the lens focal point position with respect to the target surface. *Laser Part. Beams* **26**, 189–196.

Kasperczuk, A., Pisarczyk, T., Badziak, J., Miklaszewski, R., Parys, P., Rosinski, M., Wolowski, J., Stenz, Ch., Ullschmied, J., Krousky, E., Masek, K., Pfeifer, M., Rohlena, K., Skala, J. & Pisarczyk, P. (2007*b*). Influence of the focal point position on the properties of a laser-produced plasma. *Phys. Plasmas* **14**, 102706-1/102706-8.

Kasperczuk, A., Pisarczyk, T., Borodziuk, S., Ullschmied, J., Krousky, E., Masek, K., Rohlena, K., Skala, J. & Hora, H. (2006). Stable dense plasma jets produced at laser power densities around 10^{14} W/cm^2. *Phys. Plasmas* **13**, 062704-1/062704-8.

Kasperczuk, A., Pisarczyk, T., Borodziuk, S., Ullschmied, J., Krousky, E., Masek, K., Pfeifer, M., Rohlena, K., Skala, J. & Pisarczyk, P. (2007*a*). Interferometric investigations of influence of target irradiation on the parameters of laser-produced plasma jets. *Laser Part. Beams* **25**, 425–433.

Kolacek, K., Schmidt, J., Prukner, V., Frolov, O. & Straus, J. (2008). Ways to discharge-based soft X-ray lasers with the wavelength lambda $<$15 nm. *Laser Part. Beams* **26**, 167–178.

Lebedev, S.V., Chittenden, J.P., Beg, F.N., Bland, S.N., Ciardi, A., Ampleford, D., Hughes, S., Haines, M.G., Frank, A., Blackman, E.G. & Gardier, T. (2002). Laboratory astrophysics and collimated stellar outflows: The production of radiatively cooled hypersonic plasma jets. *Astrophys. J.* **562**, 113–119.

Mizuta, A., Yamada, S. & Takabe, H. (2002). Numerical analysis of jets produced by intense laser. *Astrophys. J.* **567**, 635–642.

Nicolai, Ph., Tikhonchuk, V.T., Kasperczuk, A., Pisarczyk, T., Borodziuk, S., Rohlena, K. & Ullschmied, J. (2006). Plasma jets produced in a single laser beam interaction with a planar target. *Phys. Plasmas* **13**, 062701-1/062701-8.

Ramis, R., Ramirez, J. & Schurtz, G. (2008). Implosion symmetry of laser-irradiated cylindrical targets. *Laser Part. Beams* **26**, 113–126.

Remington, B.A., Drake, R.P. & Ryutov, D.D. (2006). Experimental astrophysics with high power lasers and Z pinches. *Rev. Mod. Phys*. **78**, 755–807.

Schaumann, G., Schollmeier, M.S., Rodriguez-Prieto, G., Blazevic, A., Brambrink, E., Geissel, M., Korostiy, S., Pirzadeh, P., Roth, M., Rosmej, F.B., Faenov, A.Y., Pikuz, T.A., Tsigutkin, K., Maron, Y., Tahir, N.A. & Hoffmann, D.H.H. (2005). High energy heavy ion jets emerging from laser plasma generated by long pulse laser beams from the NHELIX laser system at GSI. *Laser Part. Beams* **23**, 503–512.

Shigemori, K., Kodama, R., Farley, D.R., Koaste, T., Estabrook, K.G., Remington, B.A., Ryutov, D.D., Ochi, Y., Azechi, H., Stone, J. & Turner, N. (2000). Experiments on radiative collapse in laser-produced plasmas relevant to astrophsical jets. *Phys. Rev. E* **62**, 8838–8841.

Sizyuk, V., Hassanein, A. & Sizyuk, T. (2007). Hollow laser self-confined plasma for extreme ultraviolet lithography and other applications. *Laser Part. Beams* **25**, 143–154.

Wen, S.-B. & Mao, X. (2007). Expansion of the laser ablation vapor plume into a background gas. I. Analysis. *J. Appl. Phys*. **101**, 023114-1/023114-13.

Yu, W., Yu, M.Y., Xu, H., Tian, Y.W., Chen, J. & Wong, A.Y. (2007). Intense local plasma heating by stopping of ultrashort ultraintense laser pulse in dense plasma. *Laser Part. Beams* **25**, 631–638.